Transparent Earth

Remote Sensing for Mineral exploration in Zambia, 41055HQLEL

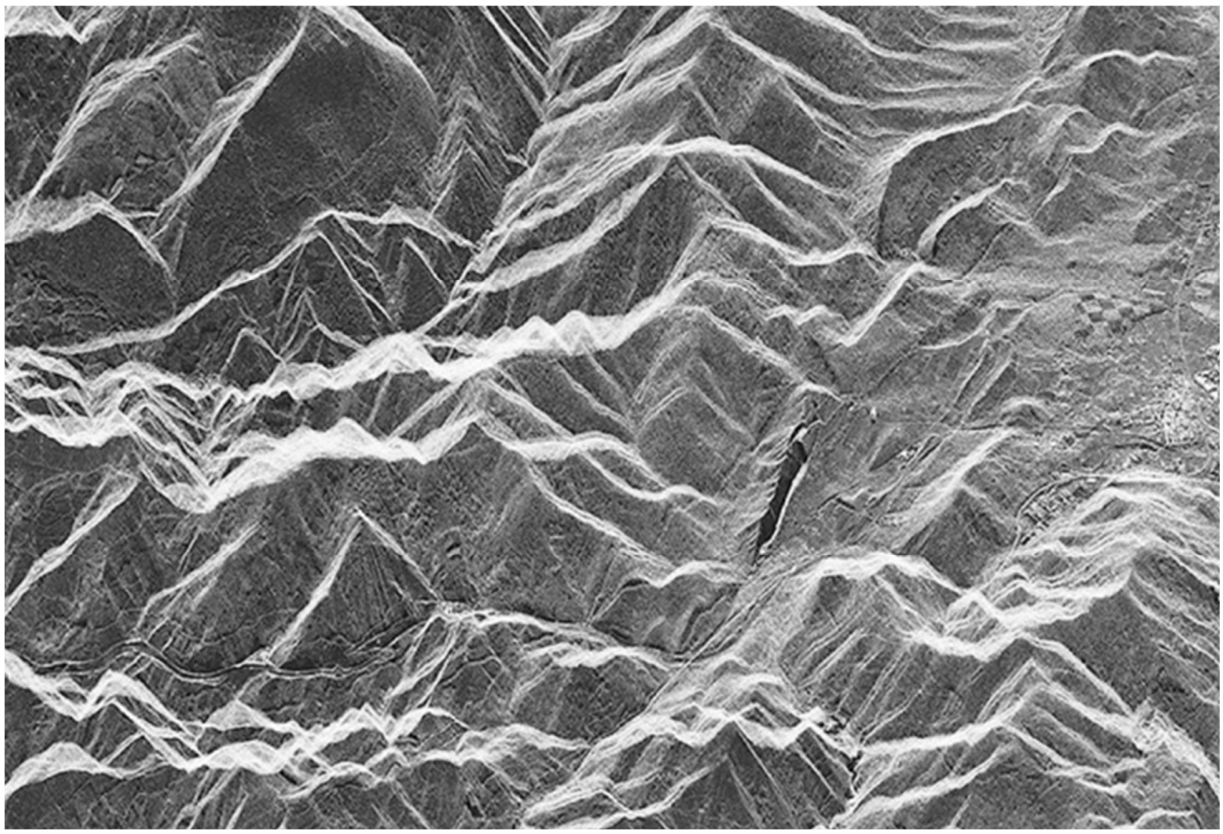

info@transparentearth.tech

Introduction

The study area comprises polygon 41055HQLEL, covering 426.5 km², with principal targets of gold, copper and zinc.

This report aims to integrate geological, geomorphological and remote-sensing analyses in support of reconnaissance exploration within the licence area. The investigation seeks to characterise the regional and local geological framework, assess structural and lithological controls on potential mineralisation, map surface morphology and drainage patterns, and apply spectral-index and spectral-unmixing methods to identify alteration signatures that may indicate gold, copper or zinc deposits.

This report offers a high-level overview of remote-sensing support for mineral exploration, grounded in a priori data review, general contextual studies, digital-elevation-model analysis, and other preparatory steps. Although the workflow is rigorous, the results remain provisional: data gaps, residual errors, and interpretive biases can persist, so field checks and iterative updates are essential. The AI-generated spectral-unmixing maps specifically assume that each pixel captures a linear mix of surface spectra, an oversimplification that may break down in heterogeneous or rugged terrain; treat them as guidance, not as definitive answers.

The report is structured as follows: Chapter 1 presents general information on location, infrastructure and land cover; Chapter 2 reviews lithology, stratigraphy and structural framework; Chapter 3 describes topography, geomorphic features and slope-related access constraints; Chapter 4 outlines remote-sensing data acquisition, preprocessing and spectral-index analysis; Chapter 5 details spectral-unmixing methodology and results; and a concluding section synthesises findings and proposes recommendations for field validation and follow-up.

General Information

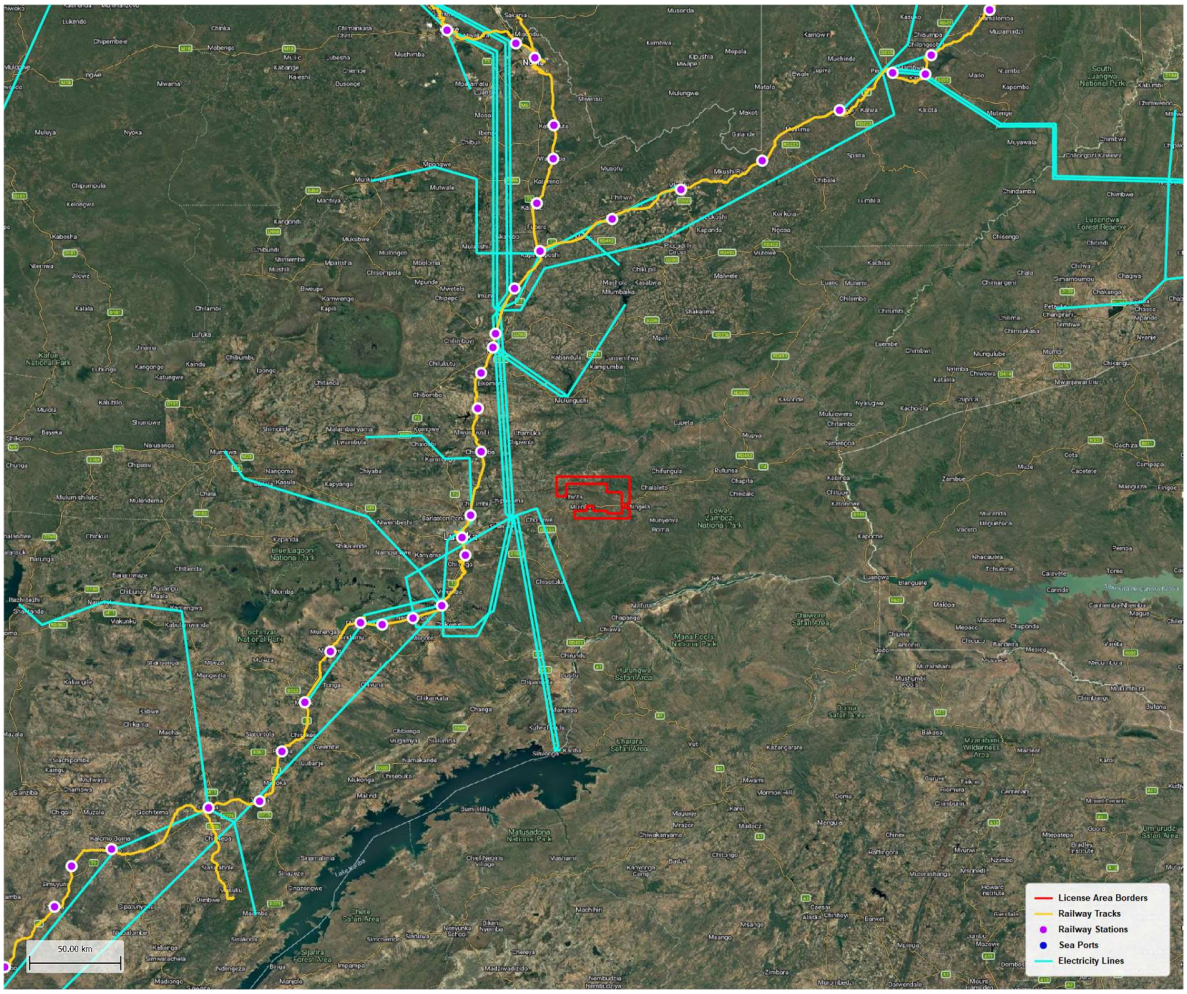

Figure 1. Overview image of 41055HQLEL in Zambia (zoom out)

Polygon 41055HQLEL displays a mosaic of smallholder farmland and remnant savanna woodland. Vegetation cover is generally sparse to moderate, with large patches of cultivated fields forming a light-toned checkerboard across the central and southern portions. A northeast–southwest ridge in the north shows denser tree cover and intermittent outcrops of weathered bedrock. Several rural hamlets—such as Chiota, Mulofwa and Undaunda—are dispersed throughout the polygon, interlinked by informal tracks.

The principal exploration targets within this license are gold, copper and zinc. These commodities are typical of the regional geologic terrane but no direct mineral occurrences are discernible in the imagery.

Surface access is excellent by road: the sealed T4 highway bisects the polygon east–west, and an intricate network of unsealed feeder roads and vehicle tracks connects local settlements and fields. There are no visible airstrips or navigable waterways. The nearest major city is Lusaka, approximately 70 km to the west by road.

No clear signs of historical or current mining—such as pits, waste dumps or stockpiles—are apparent in the imagery, suggesting that the area has not hosted significant mechanized extraction to date.

Within the polygon boundary, the mapped road network totals 409.24 km, corresponding to approximately 79.59% of the license being within 3 km of a roadway. This reflects both the highway corridor and dense agricultural access tracks.

Large-scale logistics by rail and sea are limited. There are no railway lines inside the polygon; the closest track lies 40.63 km to the north, with the nearest railway station 43.99 km away. The nearest seaport on the Indian Ocean coast is some 786.35 km distant. Electricity infrastructure also lies outside the license, with the nearest high-voltage transmission line about 12.87 km from the boundary.

Overall, polygon 41055HQLEL benefits from robust road connectivity and proximity to Lusaka, facilitating mobilization of exploration personnel and light equipment. However, bulk transport of concentrate would require long road haulage or access to railhead infrastructure over 40 km away. Extension of power lines by roughly 13 km will be necessary for any permanent camp or processing facilities, and the absence of nearby mining support services will require significant site establishment planning.

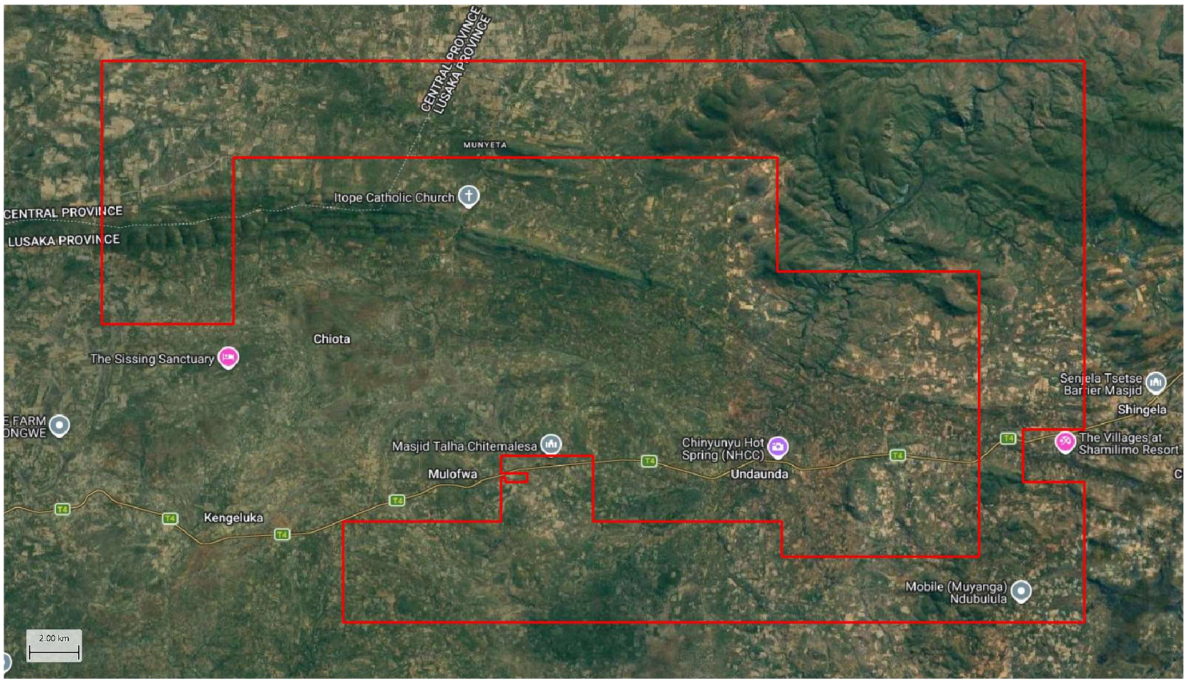

Figure 2. Overview image of 41055HQLEL (zoom in)

Geological Context

Source Inventory. The study area is located in Zambia and comprises a single polygon, 41055HQLEL, with an area of 426.5 km². The only geological source is the Geological Map of the Republic of Zambia (1981), scale 1:1 000 000, published in 1981; source type: national geological map.

Lithology & Stratigraphy. Bedrock within the polygon is entirely Precambrian in age, dominated by metamorphosed pelite–quartzite–psammite sequences (unit 15) occupying ~60% of the mapped area. Subordinate exposures of undifferentiated Basement Complex gneiss and migmatite (unit 12) cover ~20%, while elongate lenses of meta-quartzite (unit 8) and acidic metavolcanic rocks (unit 11) each occupy ~10%. No Karoo or younger sedimentary units or Quaternary cover are shown, and no unconformities are explicitly delineated within the mapped area.

Structural Framework. The polygon is transected by a series of predominantly NW–SE-trending faults, with minor NE–SW splays evident. Fault linework includes both observed and concealed segments, and a few thrust or reverse-fault symbols appear along major contacts. No fold hinges or systematic fold trends are annotated, and the map provides insufficient cross-cutting data to resolve discrete deformation phases or kinematic sequences.

Mineral Occurrences & Genetic Links. No gold, copper or zinc occurrences are mapped within or within 25 km of the polygon on the supplied mineral-deposit layers. The supplied materials do not show any labelled or symbolled mineral occurrences or alteration zones relevant to the target commodities.

Exploration Implications. The absence of surficial cover and dominance of exposed Precambrian basement afford unimpeded geological mapping and rock sampling. The intersection of meta-quartzite and metavolcanic bodies with major fault corridors presents structural targets for vein-hosted mineralisation, although no known occurrences are recorded. In the absence of mapped mineralisation, initial reconnaissance should focus on structural intersections and lithological contacts within the deformational network.

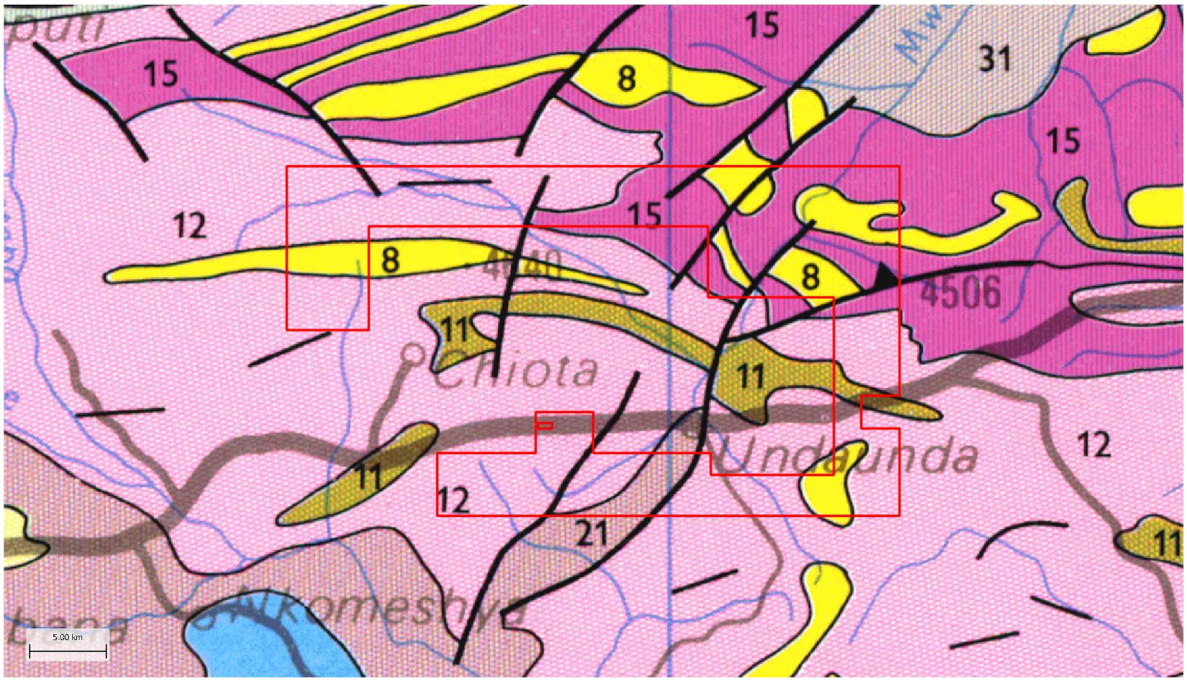

Figure 3. Geological map showing lithological units and known mineral occurrences in 41055HQLEL area

Topography and Geomorphology

DEM statistics show a maximum elevation of 1 419 m and a minimum of 615 m, yielding a relief of 804 m. The terrain transitions from a moderately dissected highland in the northeast to an undulating lowland plain south and west of the central ridge.

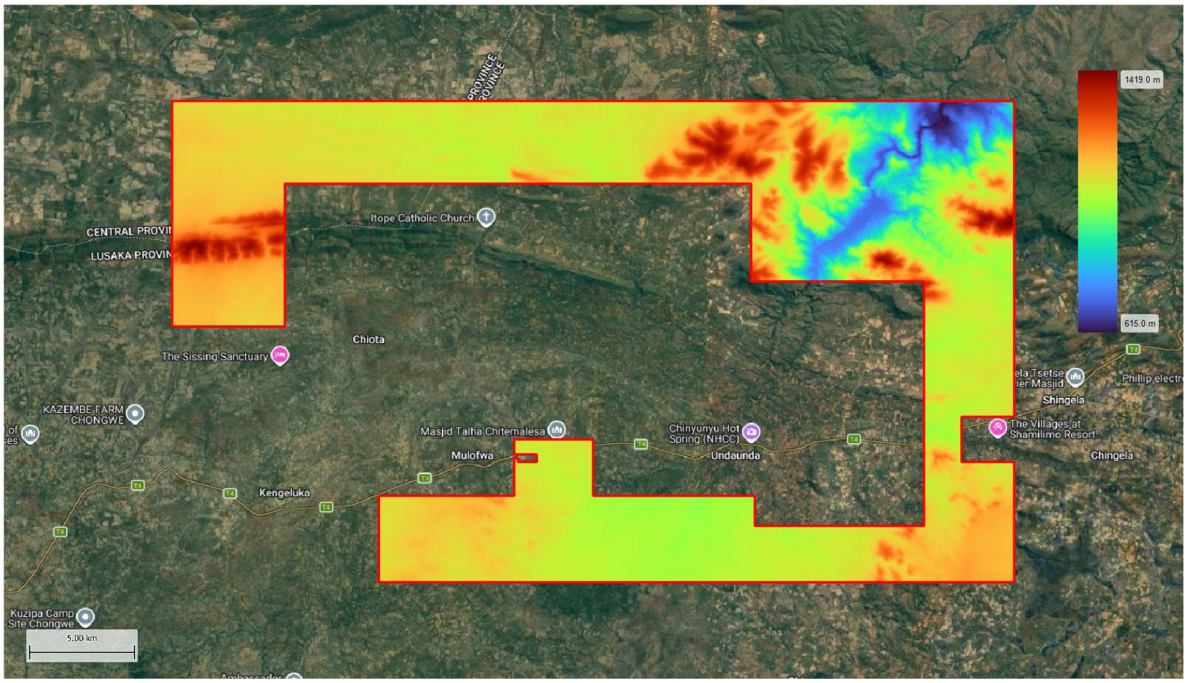

Figure 4. Digital elevation model in the 41055HQLEL.

Macro-landforms include an east–west trending highland plateau capped at ~1 400 m in the northeast, featuring crenulated ridges and narrow spurs visible on hillshade. South of this plateau, slopes drop steeply to a lower undulating plain around 700–900 m, with broad interfluves and shallow valleys. Drainage on the plateau is dendritic and entrenched, while the lower plain exhibits sparse, ephemeral channels.

The pronounced escarpment bounding the plateau suggests a lithological or structural contact, possibly a fault-controlled ridge. Aligned ridgelines and straight valley segments may reflect underlying joint sets or competent lithologies, although detailed mapping is required to confirm these controls.

Average slopes of ~7° mask local gradients exceeding 20° on the escarpment flanks. Steeper slopes will limit vehicular access and necessitate foot or winch-supported operations but offer thinner soil cover and enhanced bedrock exposure for outcrop sampling. In contrast, gentler slopes on the lowland plain support easier access but host thicker colluvial deposits that may obscure bedrock and require auger drilling to reach primary lithologies.

Present hydrological features are dominated by seasonal streams incising shallow channels, with minor terraces along valley flanks suggesting episodic base-

level changes. These terraces may concentrate placer-type gold and serve as low-energy depositional traps for heavy minerals derived from the highland.

Infrastructure mapping reveals the T4 sealed highway crossing the mid-section, providing primary east–west access. Secondary farm tracks and a dirt road ascending to the ridge crest near Itopo Catholic Church intersect moderate slopes (<15°), indicating practical routes for light vehicles. Scattered villages and fields on the lower plain offer staging points but may constrain large-scale drill access.

Overall, the terrain offers favorable conditions for structural and lithological targeting along ridge crests, where bedrock is exposed and mapping can proceed with minimal overburden. However, deep colluvial cover in valleys and steep escarpment segments will pose logistical challenges for heavy equipment and may require targeted geophysical or shallow drilling campaigns to test concealed mineralization.

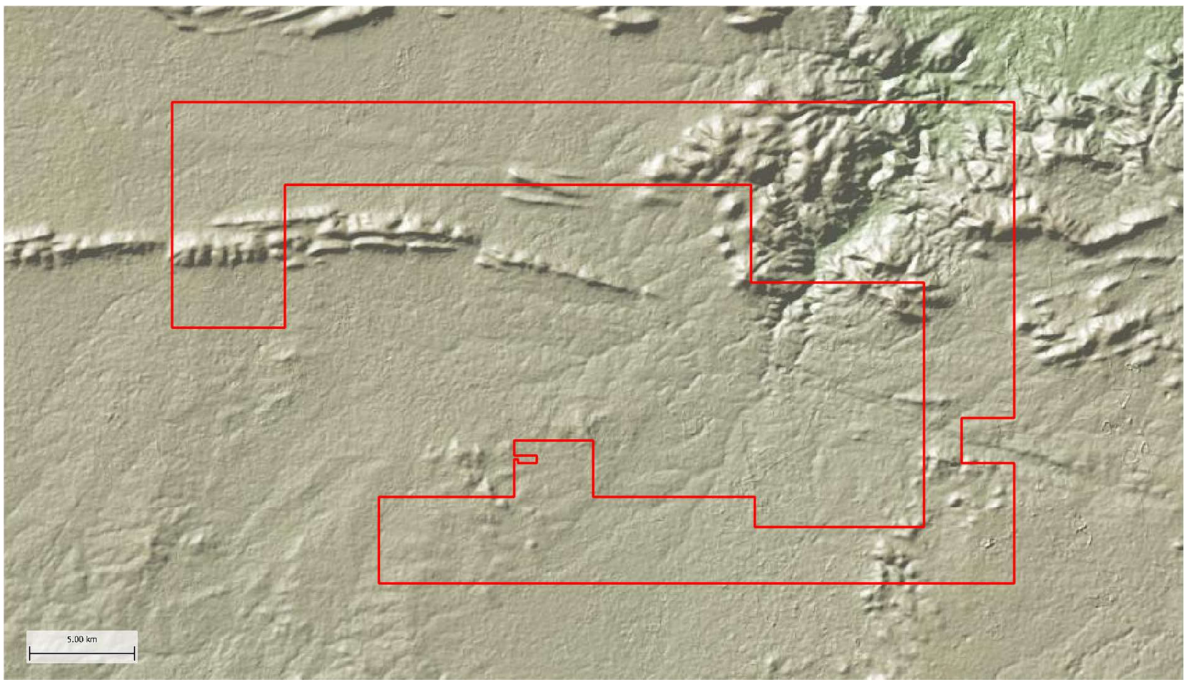

Figure 5. GMRT (Global Multi-Resolution Topography) Synthesis map for the 41055HQLEL.

Remote Sensing Basic Processing

This chapter evaluates remote-sensing data over one exploration polygon (ID 41055HQLEL) in Zambia, covering an area of 426.5 sq km. The work targets gold, copper, and zinc mineralization.

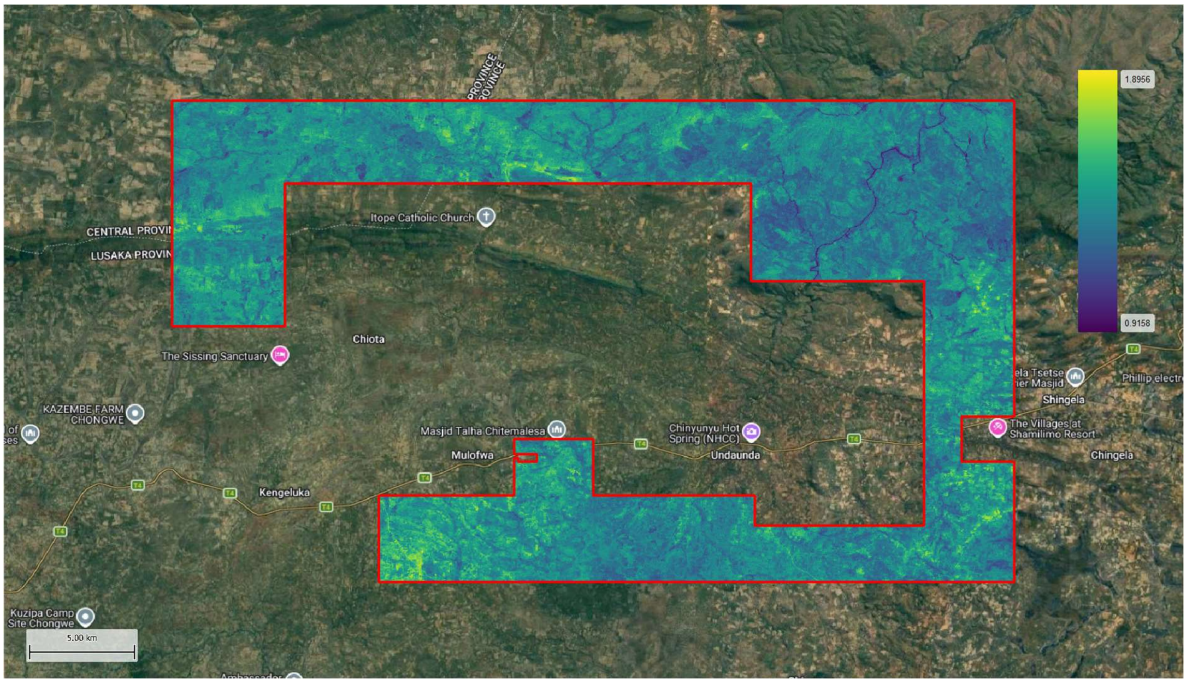

Figure 6. Iron-oxide index image obtained from modern imaging satellite

The analysis employs cloud-filtered Sentinel-2 Level-2A surface reflectance composites for the dry-season period, orthorectified and topographically corrected via SRTM-based illumination normalization. Visual inspection indicates minimal residual cloud or shadow effects and clear surface reflectance across the footprint.

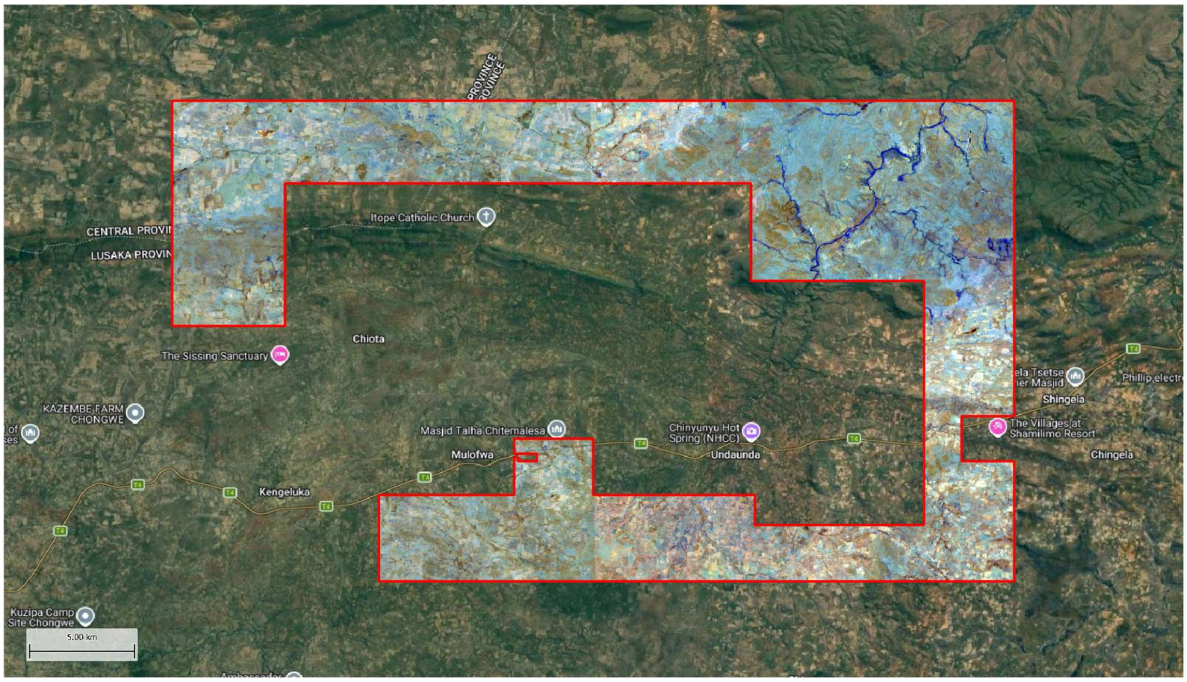

Figure 7. Modern imaging satellite near-infrared bands in RGB

Spectral-index distributions within 41055HQLEL show an iron-oxide index mean of 0.612 (= 0.689), ranging 0.0–1.896, with an anomaly threshold of 1.503 exceeding ~5% of pixels. The ferrous-silicate index averages 0.350 (= 0.395; max 1.827) with a 0.866 threshold also at ~5% exceedance. The clay/hydroxyl index has mean 0.522 (= 0.589; max 1.582), anomaly cutoff 1.313 (5% exceedance). Background index levels reflect widespread lateritic surfaces and minimal deep alteration.

On the iron-(red)/clay-(green)/ferrous-(blue) composite, discrete red-orange zones occur on gently sloping plateau crests in the northwest, coincident with iron index >1.503. Green to yellow halos in the south-central belt reflect localized clay enrichment above 1.313, while sporadic blue-cyan pixels along ephemeral drainage lines indicate elevated ferrous silicates above 0.866. Extensive, diffuse iron signatures on plateau margins correspond to known lateritic lag rather than hydrothermal caps. Patches where iron and clay anomalies overlap (central valley and south edge) are most suggestive of hydrothermal argillic alteration, but they cover <2% of the area and require ground confirmation. Terrain slopes average <10°, with no clear linear alignments between spectral anomalies and major DEM lineaments. Vegetation cover is minimal (mean NDVI 0.081), with <0.01 proportion of pixels showing NDVI > 0.5, so masking of spectral signals is negligible; ephemeral wet zones along drainage produce limited NDWI anomalies but do not significantly impact index mapping. Two clusters with co-occurring iron and clay anomalies are ranked as Tier-1 priority, while isolated iron-only zones are designated Tier-2.

These remote-sensing results guide field planning by focusing soil sampling and systematic mapping on Tier-1 clusters where index co-occurrence may mark hydrothermal alteration. Shallow auger or trench sampling should target south-central and central valley overlaps, with scout RC drilling prioritized on accessible river

terrace exposures. Tier-2 iron-only anomalies are second-priority and warrant follow-up after principal cluster evaluation.

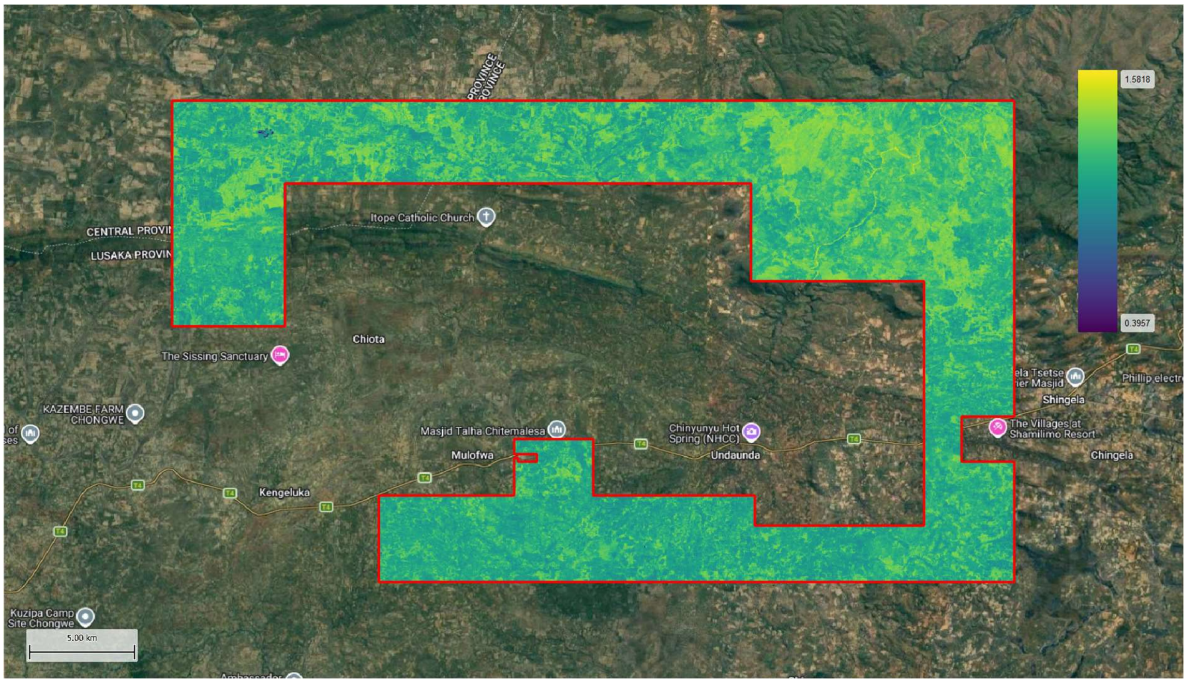

Figure 8. Clay-hydroxyl index image obtained from modern imaging satellite

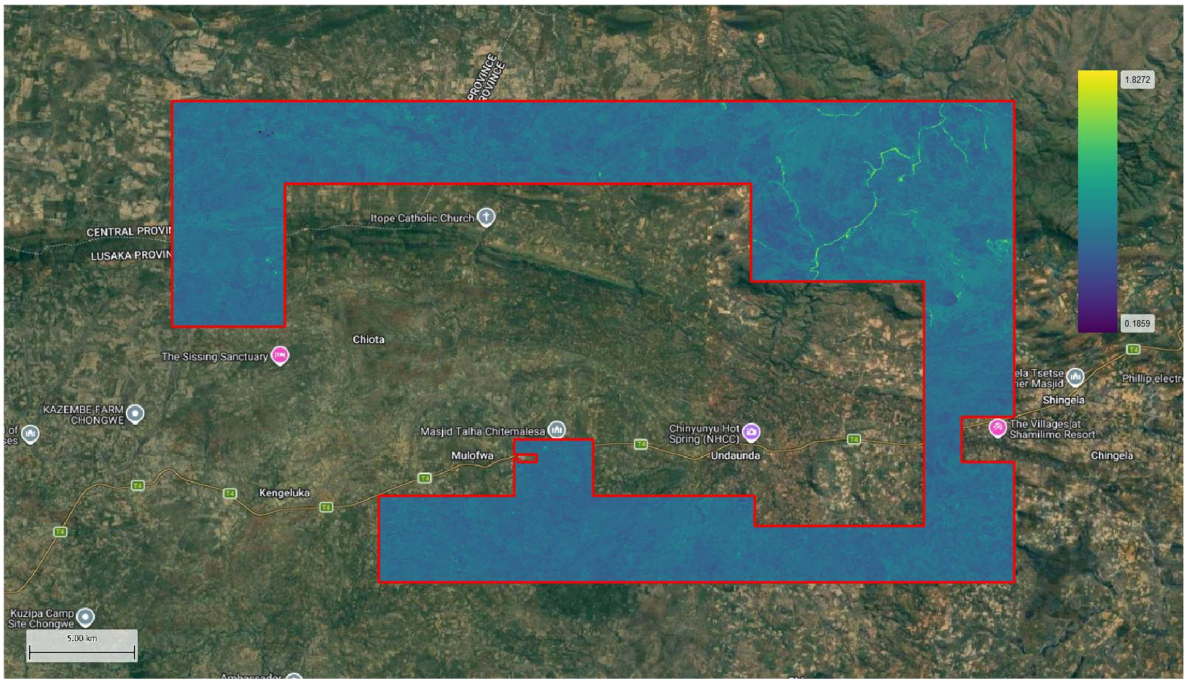

Figure 9. Ferrous-silicate index image obtained from modern imaging satellite

Application of Spectral Unmixing

Spectral unmixing is a widely used remote sensing technique crucial for identifying prospective mineral areas within our study region in Zambia. The key assumption behind this method is that the signal received by the satellite — orbiting about 786 km above Earth — is a linear spectral mixture of reflected signals from each 10*10 m pixel: vegetation, water, soil, and, ideally, minerals of interest. By relying on distinct mineral signatures (reflectivity spectra) and applying necessary atmospheric corrections, we can decompose the satellite image data into detailed mineralogical maps.

Figure 8 illustrates the basic idea: each pixel in a satellite image contains a "signature" of various wavelengths of light, which is essentially a linear mixture of signatures from different materials. By carefully analyzing these signatures, we can determine which materials are present — even if they're mixed together. This process is known as spectral unmixing.

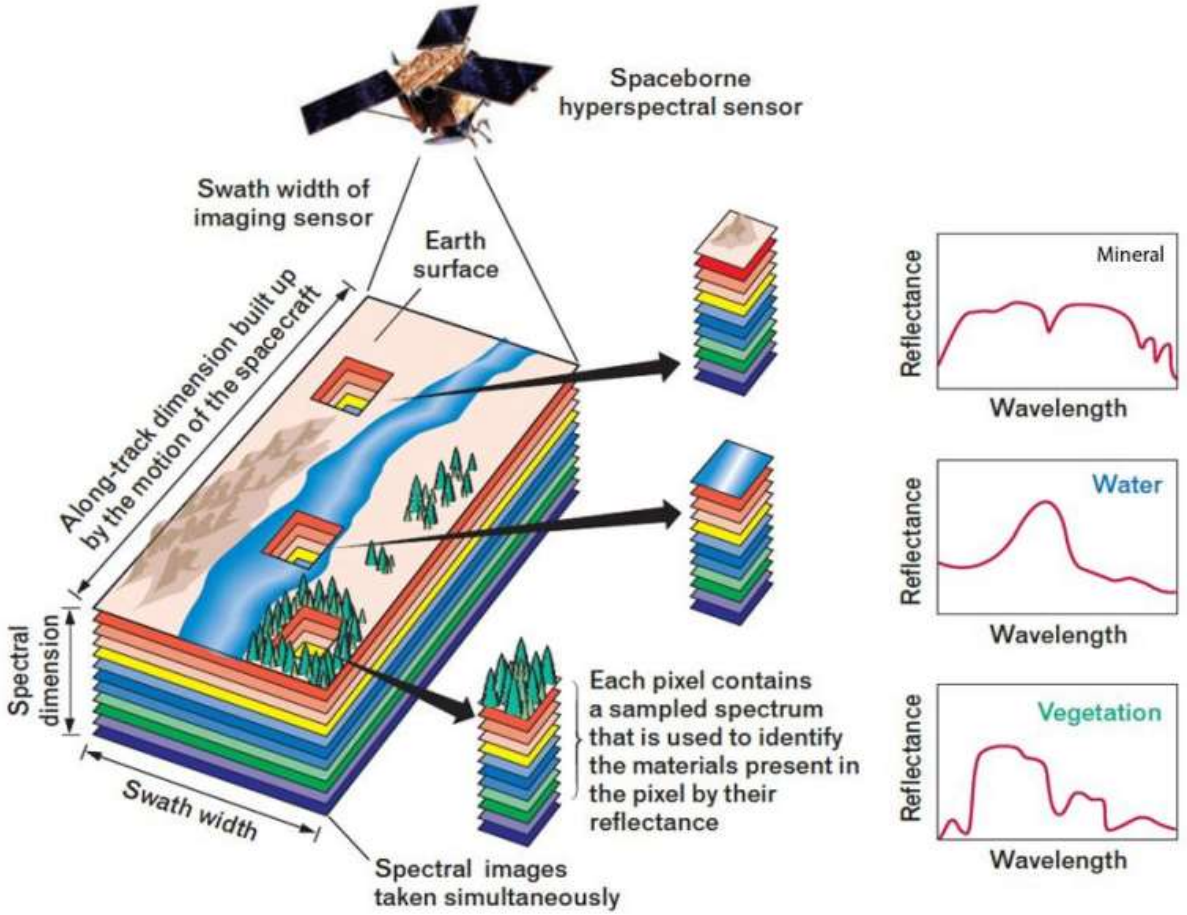

Figure 10. Spectral unmixing basic principles illustrated.

Although non-linear mixing may occur in certain conditions, spectral unmixing has become a powerful tool in mineral exploration, making it easier, faster, and more

cost-effective than traditional methods alone. While dense vegetation and residual atmospheric effects can obscure underlying geological features, spectral unmixing remains invaluable for making initial estimations of mineral presence.

For this analysis, we utilized recent state-of-the-art satellite mission images captured in 2025, each covering an area of approximately 100x100 km. These images provide the high-resolution multispectral data necessary for accurate spectral unmixing, despite the challenges posed by the vegetation cover.

The spectral unmixing process involved comparing the satellite data with spectral signatures of minerals obtained under laboratory conditions. These signatures, representing the reflectance of minerals across various wavelengths in the visible (VNIR) and short-wave infrared (SWIR) ranges, serve as benchmarks for the satellite data comparison.

The full list of minerals considered in our spectral unmixing analysis included chalcopyrite, pyrite, sphalerite, serpentine, quartz, pyroxene, orthoclase, olivine, magnetite, kaolinite, hematite, goethite, galena, dolomite, chlorite, calcite, biotite, amphibole, and a special endmember for vegetation to account for its reflectivity. The spectral signatures for these minerals were sourced from the USGS Spectral Library (Kokaly et al., 2017).

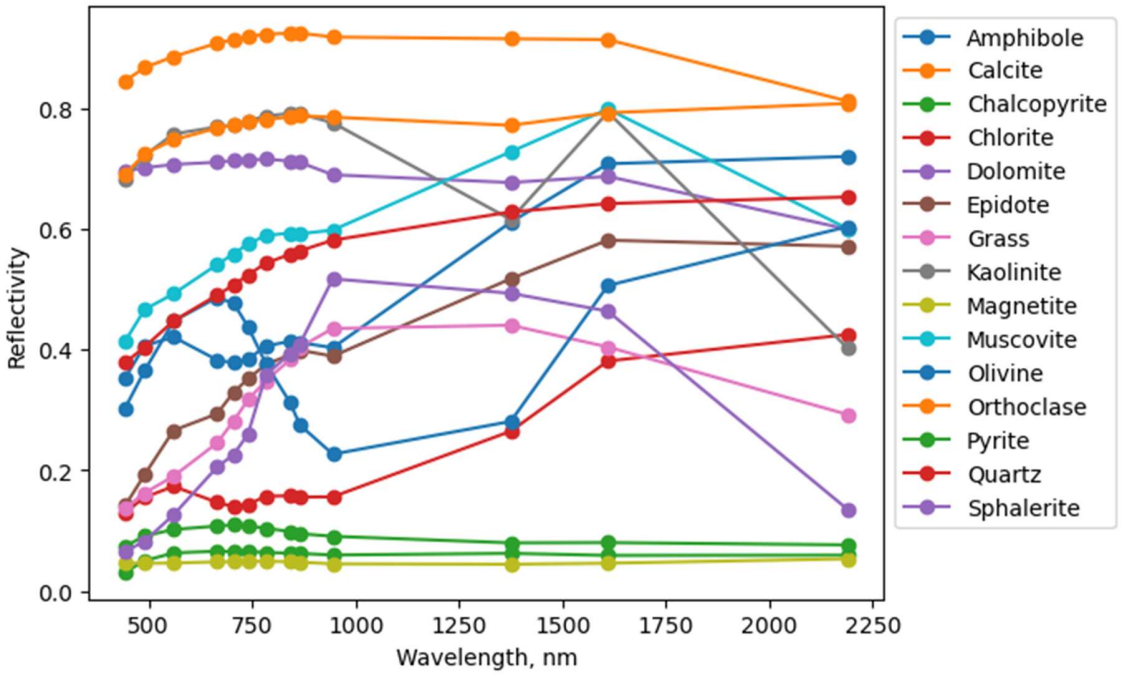

Figure 11. Spectral signatures for selected minerals.

AI-Spectral Unmixing Methodology

Following the spectral unmixing framework introduced in the previous chapter, we now implement a novel methodology that utilizes generative deep learning to enhance mineral prospecting. Neural Networks have witnessed a surge in applications across various fields, demonstrating their versatility and power in tackling complex problems. In the domain of remote sensing and mineral exploration, NNs offer substantial benefits by enabling the handling of large datasets, automating pattern recognition, and providing a level of analysis depth previously unattainable with traditional methods.

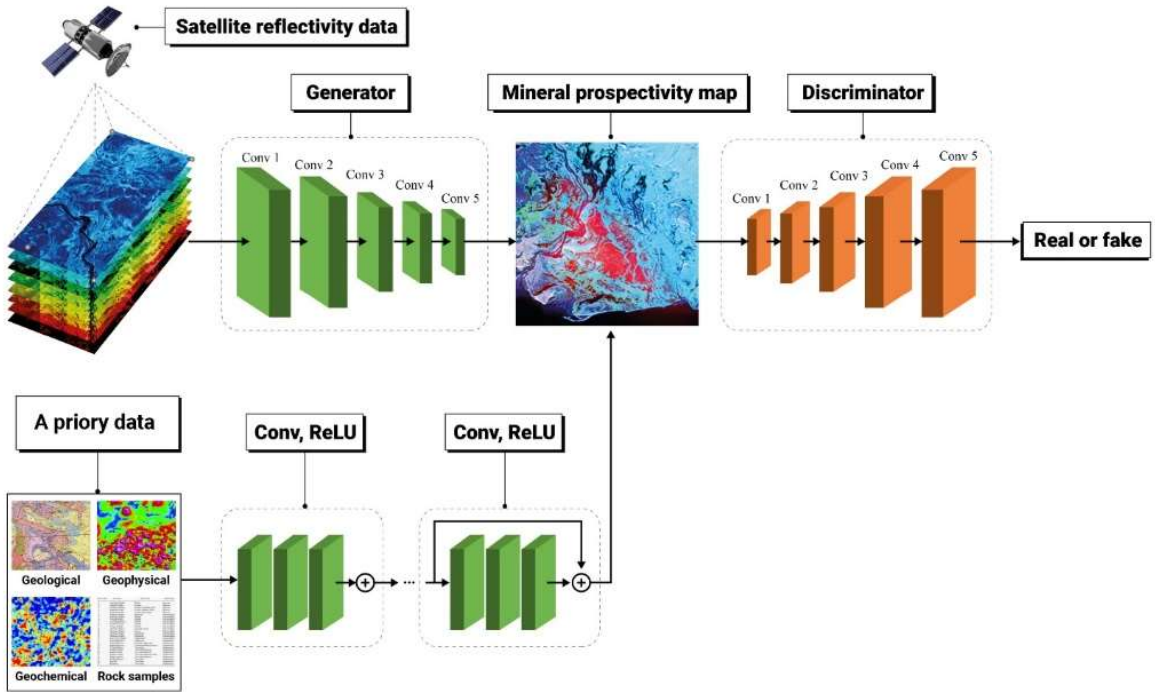

Figure 12. Schematic representation of a GAN-based mineral prospectivity mapping workflow.

At its core, the approach integrates the unmixed mineral signatures from satellite reflectivity data with a wide range of ancillary geospatial inputs. These can include geological maps, geophysical surveys, geochemical analyses, rock sample datasets, elevation models, and other a priori data. Although some of these sources may occasionally be missing or incomplete, the flexibility of this neural network architecture allows for robust mineral prospectivity mapping even when certain inputs are absent. The spectral unmixing outputs, however, remain a key component of the workflow, providing critical information about the distribution of individual mineral endmembers on the surface.

The system's underlying mechanism is a Generative Adversarial Network (GAN) that consists of a Generator and a Discriminator. During the training phase, the Generator accepts two streams of information: satellite reflectivity data (processed to

separate out mineral-specific signals) and the various convolutionally processed a priori data layers. By fusing these inputs, the Generator produces synthetic mineral prospectivity maps, which the Discriminator then evaluates as either “real” or “fake.” Through iterative feedback and refinement, the Generator learns to generate increasingly accurate prospectivity maps.

In practice, this workflow has been applied to our study region in Zambia using contemporary image sensor imagery from 2025, each scene covering approximately 100 × 100 km. Even in areas with dense vegetation that can obscure underlying geological features, the GAN-based method refines the spectral unmixing outputs to highlight potential zones of mineralization with far greater precision than traditional methods. The final prospectivity maps help reduce the costs and risks associated with field surveys, since geological teams can focus on the most promising targets. By combining spectral unmixing to isolate essential mineral signatures with deep generative models that incorporate other critical geospatial data, this technique sets a new benchmark in remote sensing–driven exploration, offering a powerful and efficient pathway for identifying valuable mineral deposits.

The integration of advanced satellite technology, comprehensive mineral response databases, and state-of-the-art machine learning algorithms presents a groundbreaking approach to mineral exploration. By harnessing the strengths of each component, our method facilitates the creation of detailed and predictive mineral concentration maps. These maps not only identify potential mineral deposits but also highlight the concentration and distribution of key minerals, guiding further exploration efforts with unprecedented precision.

In conclusion, the method introduced by Mikhaylov and Samsonov represents a significant leap forward in mineral exploration technology. By combining satellite spectrometry with the power of generative deep learning, it opens new avenues for accurately mapping mineral concentrations across diverse geological terrains. This development not only enhances our understanding of the Earth's subsurface resources but also sets a new standard for efficiency and accuracy in the field of geological exploration.

Spectral Unmixing Results

Introductory Paragraph. This chapter presents the spectral-unmixing results for the Zambia polygon 41055HQLEL and summarizes the spatial distribution of abundance responses observed in the six supplied figures. Each map is interpreted conservatively by direct reference to the turbo color bar ranges and the visible patterns against the Google Satellite background. The following paragraphs describe the response of each endmember across the 426.5 km² area.

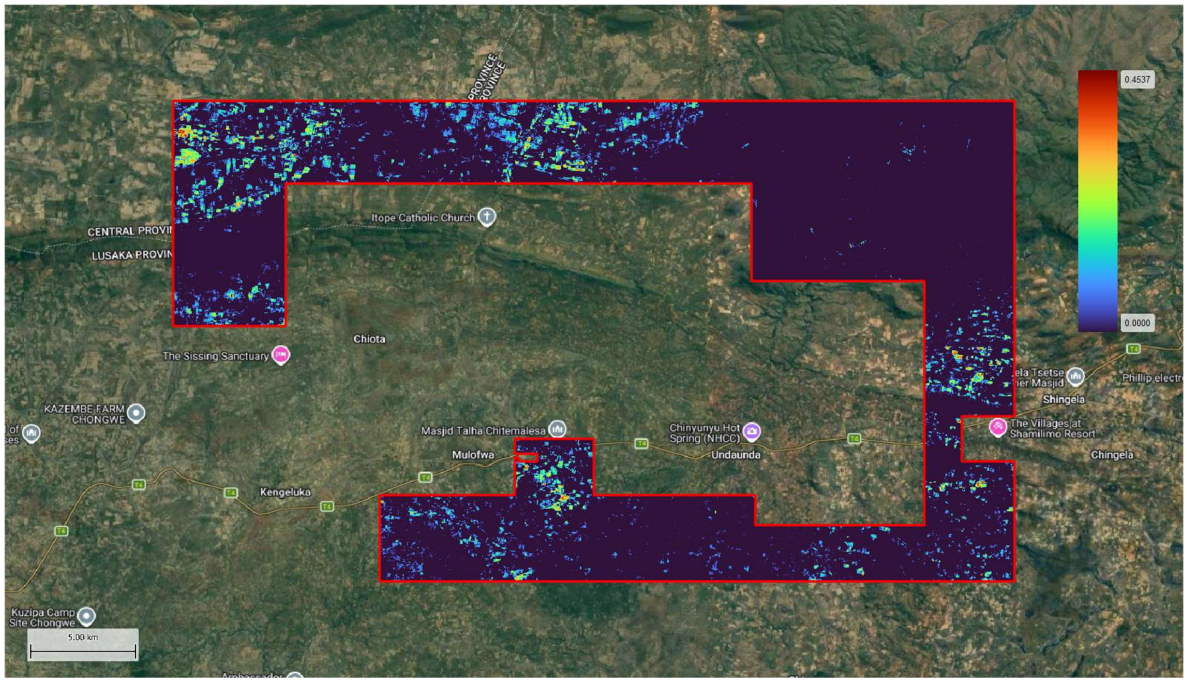

Figure 13.1. Spectral unmixing abundance map for Muscovite within the study area.

Muscovite. The muscovite response varies between 0.0000 and 0.4537. Nearly the entire polygon shows negligible to very low values (<0.05, dark purple), except for a small cluster of elevated pixels (green to yellow, ~0.2–0.4) around the central raised zone near Mulofwa. These localized anomalies coincide with rocky patches in the Google imagery but cover too small an area for definitive alteration mapping. The muscovite map suggests possible phyllosilicate occurrences that warrant field checking but remains non-diagnostic on its own.

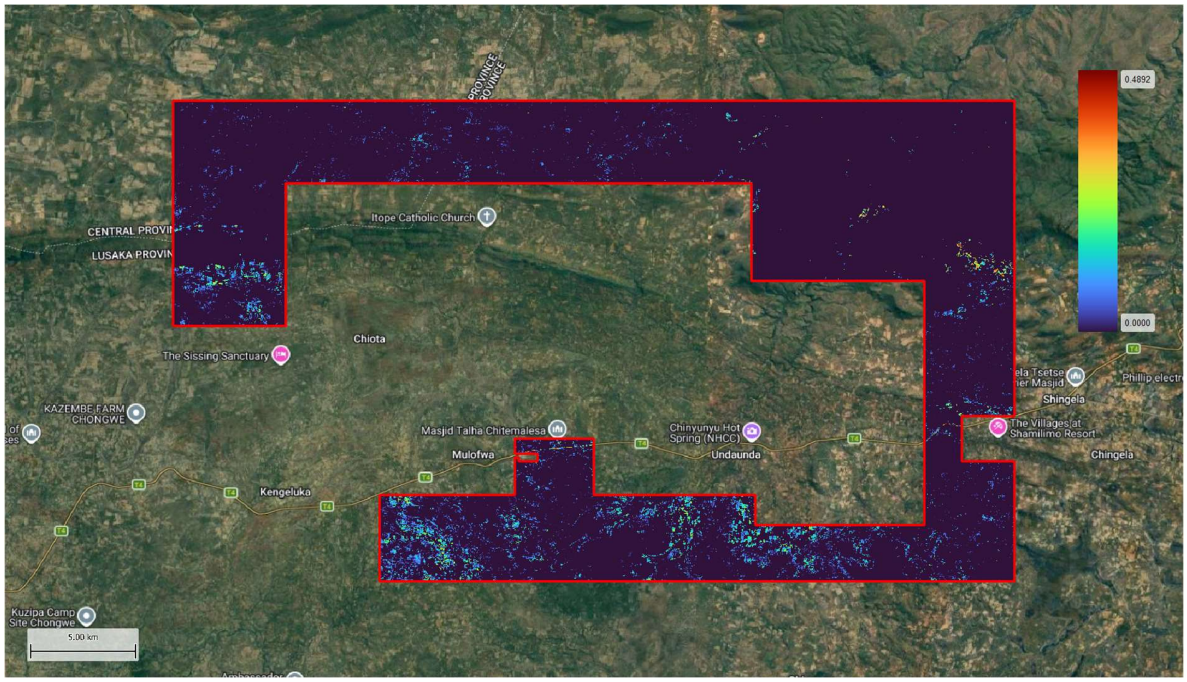

Figure 13.2. Spectral unmixing abundance map for Chalcopyrite within the study area.

Chalcopyrite. Chalcopyrite abundances span 0.0000 to 0.4892 but are overwhelmingly near zero across >95 % of the area (dark purple/blue, <0.05). Only isolated tiny clusters of weak to moderate values (light blue to green, ~0.1–0.3) appear in the southern and central sub-polygons, with no clear alignment to mapped outcrops or structural features. Overall, this map does not provide meaningful evidence for substantial chalcopyrite presence and should not be over-interpreted as a copper target.

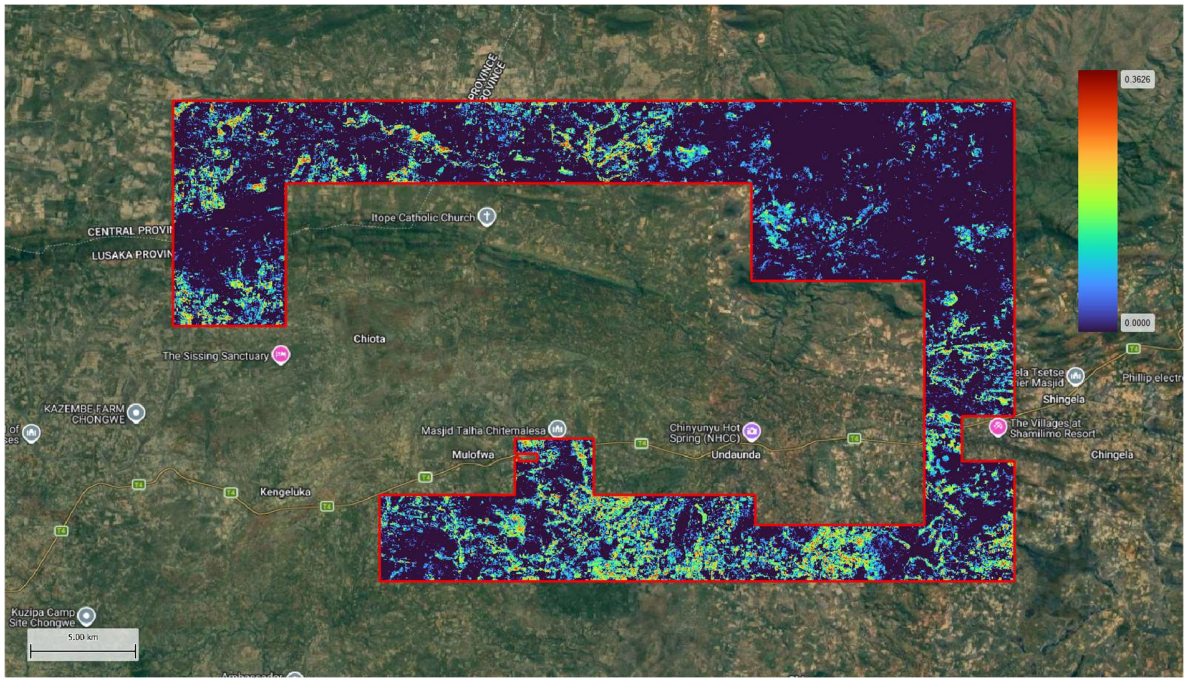

Figure 13.3. Spectral unmixing abundance map for Chlorite within the study area.

Chlorite. Chlorite abundance values range from 0.0000 to 0.3626. Most of the polygon stays below ~0.1 (dark blue/purple), though scattered clusters of light green to yellow (~0.15–0.35) appear along the southwestern and southeastern extents, correlating loosely with more rugged terrain and shadowed slopes. These limited chlorite-rich signals could reflect minor mafic alteration or vegetation interference. Given their diffuse and low-intensity nature, they require cautious follow-up rather than serving as standalone indicators of chloritic alteration.

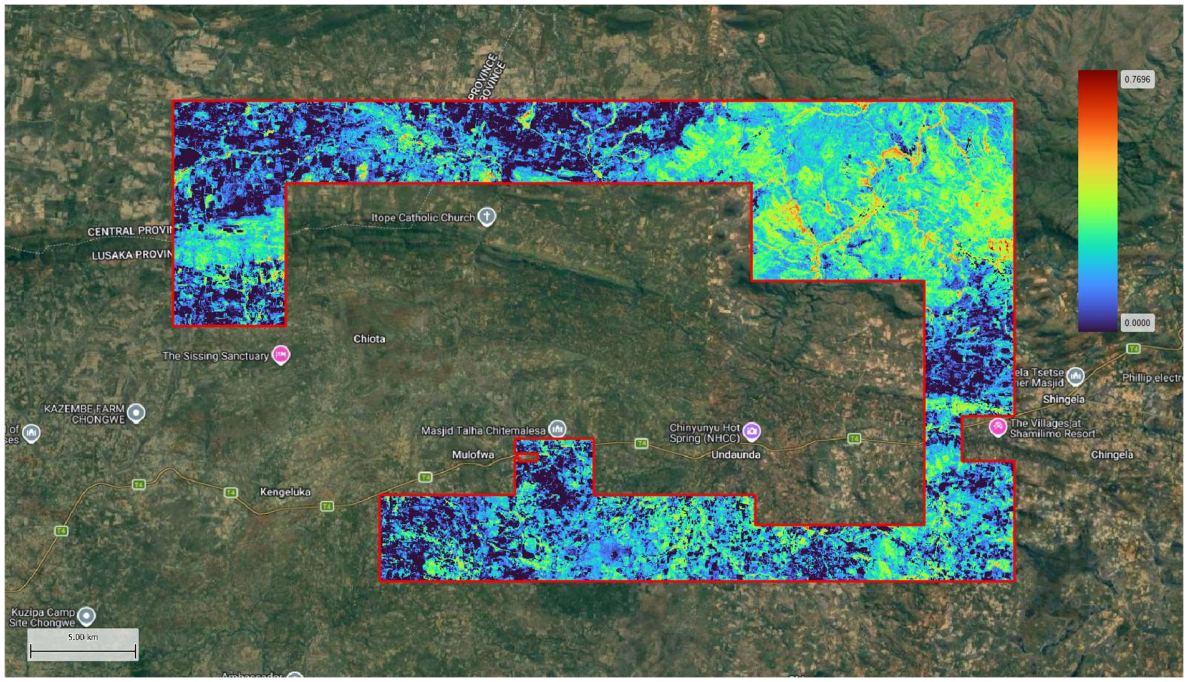

Figure 13.4. Spectral unmixing abundance map for Magnetite within the study area.

Magnetite. The magnetite abundance map ranges from 0.0000 to 0.7696. Most of the interior remains at very low values (<0.1, dark blue), with scattered patchy anomalies in the northern and northeastern edges reaching moderate to strong levels (green to red, ~0.3–0.7). These localized hotspots often align with darker hill slopes visible on the Google background. Given the restricted spatial extent of elevated magnetite signal and potential influence of surface shading or basaltic outcrops, these anomalies require cautious interpretation rather than direct evidence of magnetite-rich lithologies.

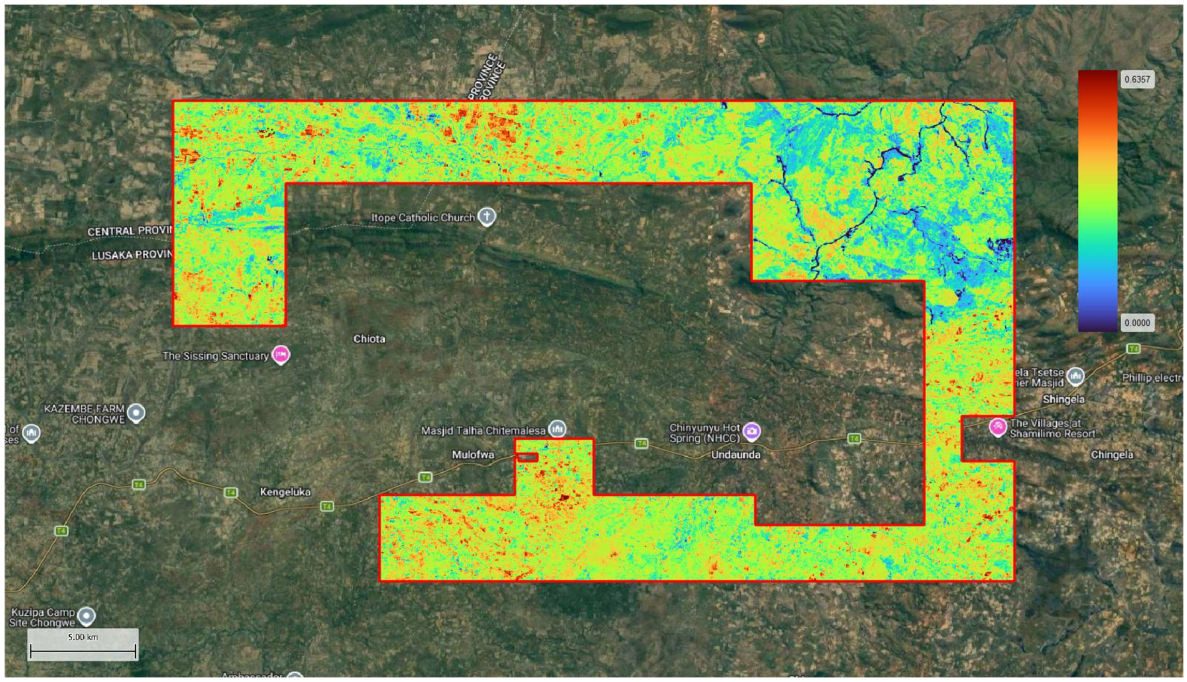

Figure 13.5. Spectral unmixing abundance map for Hematite within the study area.

Hematite. The hematite map's scale runs from 0.0000 to 0.6357. Background values cluster at low to moderate levels (blue to light green, ~0.1–0.3) across most of the polygon, while more pronounced anomalies (yellow to red, ~0.4–0.6) occur in patches along the northern boundary and within a few drainage networks in the east. These moderate hematite responses may reflect surficial ferric oxide in soils or weathered bedrock exposures visible as reddish patches in the satellite view. The pattern is too diffuse and variable to confirm a coherent mineralized zone without field verification.

Concluding Paragraph. Among the six endmember maps, the dry-grass signature is clearly an environmental effect and non-diagnostic, while chalcopyrite remains effectively absent save for a few weak isolated pixels. Muscovite and chlorite show small, localized elevated values that may hint at alteration but occupy a minor fraction of the polygon. Hematite and magnetite display more widespread moderate anomalies along edges and drainage corridors, yet these could equally reflect surficial oxides or topographic shading. All observed responses should be treated conservatively and validated through targeted field investigation before inferring geological significance.

Suggested Reconnaissance Survey Points

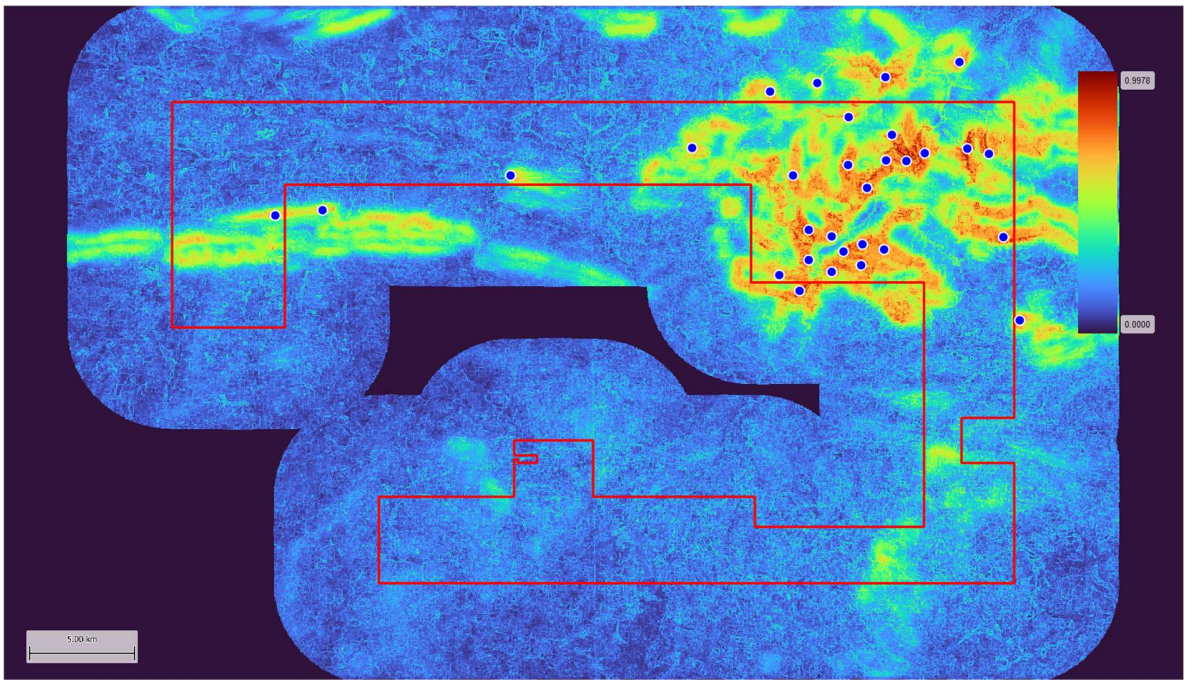

Figure 14. Suggested reconnaissance points overlaid on the remote-sensing composite. Points represent local maxima of the deterministic scoring raster after spacing and validity filters.

ROI Scoring for Mineral Exploration

Our scoring ranks polygons and mining license areas on a 0–1 scale and groups them into practical tiers: **Very High (≥0.80)**, **High (0.50–0.79)**, **Moderate (0.30–0.49)**, **Low (<0.30)**, and **Data Deficient** when inputs are unavailable. The goal is simple: give decision-makers a fast, comparable read on where effort and capital are most likely to pay off.

At its core, the system is a multifactor analysis that blends geology, geomorphology/relief, logistics and access, remote-sensing indices, and economics-adjacent considerations. Among these, a key contributor is our **technique of spectral unmixing of satellite data**. The composite score represents the coherence of evidence across all data.

Tier	Score range	Investment risk*
Very High	≥ 0.80	Lowest expected risk; advance first on current evidence.
High	0.50–0.79	Strong potential with manageable uncertainties; prioritize focused fieldwork.
Moderate	0.30–0.49	Mixed or patchy signals; medium risk—second priority or await new data.
Low	< 0.30	Weak or inconsistent signals; higher risk—deprioritize unless strategic.
Data Deficient	—	Risk unknown due to missing inputs; acquire baseline data first.

Two cautions guide our interpretation. First, a high tier is **not a guarantee** of discovery; it signals that multiple, independent lines of evidence point in the same direction. Second, results improve as new information arrives. Scores are **auditable and updatable** — when inputs change, the tiers can be refreshed without rebuilding the entire system.

In short: this scoring framework turns diverse geoscience and practical constraints into a single, transparent signal. It is designed to reduce risk, focus budgets, and keep attention on the polygons and licenses most likely to deliver value first.

Disclaimer

Geological prospectivity assessments are probabilistic. Field validation and, ultimately, drilling are required to confirm mineralization. Results depend on data availability and quality; areas may be upgraded or downgraded as new datasets are acquired.

Supporting Factor Scores

Key drivers can be grouped into four dimensions: geology, development complexity, infrastructure/logistics and legal stability. Each is expressed as an AI-derived score on a 0–100 scale, where higher values indicate more favourable conditions.

- Geology 64.4 – The geology score is moderate, with some favourable lithologies and iron anomalies present but not consistently developed across the licence.
- Development complexity 44.2 – The development-complexity score is moderate, with a mix of accessible ground and localised constraints related to relief, cover or existing workings.
- Infrastructure / logistics 90.8 – The infrastructure/logistics score is high, indicating good road connectivity and a large proportion of ground that should be accessible to light vehicles.
- Legal stability 70.0 – The legal-stability score is high, indicating a generally stable and predictable legal and policy environment for mining investment.

Fieldwork Seasonality

Area: 41055HQLEL, Zambia. This climatological assessment supports planning of geological mapping and surface sampling. It uses monthly precipitation and average daily minimum and maximum temperatures.

Preferred field period: April–September. **Preferred months:** Apr, May, Jun, Jul, Aug, Sep. **Workable shoulder months:** Mar, Oct, Nov. The main climatic constraints are rainfall.

Score interpretation: 0–100; higher is better. The total score combines 50% precipitation + 30% daytime temperature + 20% cold-night temperature. A weak component or an extreme temperature can cap the rating.

Month	Rainfall mm	Tmin °C	Tmax °C	Score	Rating
January	214.0	17.6	26.8	58.4	Difficult
February	174.0	17.5	27.0	64.4	Difficult
March	104.0	16.6	27.2	76.7	Workable
April	**37.0**	**14.6**	**27.1**	**95.6**	**Preferred**
May	**8.0**	**11.4**	**25.9**	**99.7**	**Preferred**
June	**0.0**	**8.7**	**24.0**	**99.4**	**Preferred**
July	**0.0**	**8.3**	**24.0**	**99.4**	**Preferred**
August	**0.0**	**10.6**	**26.8**	**99.8**	**Preferred**
September	**1.0**	**14.6**	**31.0**	**95.5**	**Preferred**
October	15.0	17.7	32.7	90.4	Workable
November	72.0	18.3	30.9	81.7	Workable
December	208.0	17.8	27.4	59.1	Difficult

Climate source: WorldClim historical climate 2.1; reference period 1970-2000; nominal resolution 2.5 arc-minutes (approximately 4-5 km at the equator). This is a long-term climatological planning aid, not a forecast. It does not directly model snow cover, flooding, road condition, vegetation, security, permits or local access restrictions.

Conclusion

The intersection of NW–SE fault corridors with quartzite–pelite sequences and acidic metavolcanic lenses provides structural traps conducive to gold mineralisation and potential copper and zinc deposition. Spectral-index anomalies, notably co-located iron and clay anomalies on plateau margins and central valleys, confirm limited hydrothermal alteration consistent with this model.

The top decile of combined spectral anomalies covers ~8.5 km² (2.0 % of the licence) while above-median spectral-index areas encompass ~213 km² (50.0 %). The highest-ranked Tier-1 cluster lies approximately 2 km from the sealed T4 highway.

Road connectivity is excellent, with the sealed T4 highway bisecting the licence, an extensive network of unsealed tracks, sparse vegetation cover and multiple feeder roads providing light-vehicle access to ridge crests. However, steep escarpment slopes exceeding 20° on the plateau flanks present a significant operational constraint for heavy drilling and equipment mobilisation.

Composite AI prospectivity score: 0.71 (Tier: High). Favourable lithology, percent of 1.0 and top_decile_iron_pct of 0.1 support limited but positive hydrothermal potential. Accessibility metrics including slope_mean_deg of 7°, drivable_terrain_pct of 62 and roads_coverage_pct of 79.59 % with road_distance_km of 0.0 underline operational readiness. Cost variables such as distance_to_sea_port_km of 786.35 km and min_distance_to_railway_track_km of 40.63 km temper these advantages; this quantitative view complements rather than replaces geological judgement.

Used scoring parameters:

Parameter name	Interpretation	Value
Favourable lithology, percent	benefit	1.0
Top decile iron, percent	benefit	0.1
Relief range, m	cost	804
Mean slope, degrees	cost	7
Drivable terrain (<5°), %	benefit	62
Distance to nearest road, km	cost	0.0
Road coverage within polygon, %	benefit	79.59
Distance to nearest railway track, km	cost	40.63
Distance to nearest railway station, km	cost	43.99
Distance to nearest sea port, km	cost	786.35
Distance to nearest electricity transmission line, km	cost	12.87

Best unit favorability (0–10)	benefit	6
Visible mining activity (0–10)	benefit	0
Vegetation cover, percent	cost	0.0
Polygon area, sq km	benefit	426.5

Total score: 0.707

Interpretive consequence. The High-tier classification supports prioritising 41055-HQ-LEL for focused field investigation. It should not be read as high confidence that an economic deposit is already present.

Additional research and the KUMBA study

The KUMBA technical study adds useful regional and structural context and identifies several named mineral occurrences, prospective structural corridors and target zones that can be used as hypotheses for field testing. This information is potentially important, particularly where it suggests specific local targets that were not available in the original source inventory. However, the two desktop evidence sets are not yet fully reconciled. In particular, KUMBA reports local occurrences that are absent from the original mineral-occurrence layers; their coordinates, source provenance and relationship to the legal licence boundary should therefore be independently verified before they are treated as direct licence evidence.

KUMBA also models an exploration area of approximately 36,520 ha (about 365 km^2), whereas the present report uses a licence area of 426.5 km^2. This difference is material for target counts, areal percentages and any licence-wide extrapolation. The model boundary and the authoritative licence polygon should be reconciled before KUMBA-derived spatial statistics are incorporated quantitatively into the current report.

The strongest parts of the KUMBA work are therefore its regional geological compilation, structural framework and exploration-programme ideas. By contrast, the Sentinel-2 “gas anomaly” interpretation, some specific mineral-signature claims, the weakly validated machine-learning outputs, and the approximately 929 Mt conceptual mineralised-domain scenario should be treated as hypothesis-generating layers rather than independent proof. The latter figure does not represent contained metal or a Mineral Resource and is not supported by drilling, site-specific density measurements or demonstrated mineralised thickness.

Updated exploration judgement

Taken together, the current evidence supports continued prioritisation of 41055-HQ-LEL as a High-tier exploration opportunity while geological confidence remains at a reconnaissance stage. The licence has plausible structural and lithological targets, limited surface responses consistent with possible alteration, favourable regional context and strong operational access. The additional KUMBA study broadens the target-generation framework and may provide valuable specific leads, but it does not

yet demonstrate a mineralised body within the licence.

The practical interpretation is therefore field-testable prospectivity: the project merits focused expenditure to determine whether the desktop anomalies and structural hypotheses correspond to real alteration and mineralisation on the ground. At present there is insufficient evidence to make claims about grade continuity, economic tonnage, resource scale or drill-ready status across the licence.

Recommended next steps

- **Reconcile spatial datasets.** Confirm the authoritative 41055-HQ-LEL boundary and cross-check the original report, KUMBA target polygons and reported occurrences against the same licence geometry.
- **Verify the highest-value desktop leads.** Prioritise field visits where the original Tier-1 anomaly clusters, major structural intersections and credible KUMBA targets overlap or lie in close proximity. Record lithology, alteration, structure, exposure quality and evidence of workings or mineralisation.
- **Acquire controlled geochemistry.** Use systematic soil and/or regolith sampling where appropriate, plus rock-chip/channel sampling of verified exposures. Laboratory analyses and QA/QC should precede any substantial upgrade of geological confidence.
- **Apply geophysics selectively.** Use magnetics and, where sulphide or disseminated mineralisation is geologically plausible, IP/resistivity over targets supported by field geology and geochemistry rather than as blanket confirmation of model-derived anomalies.
- **Define drill targets only after convergence.** A target should be considered drill-ready when field geology, geochemistry and an appropriate structural/geophysical model define a coherent testable geometry. Ground geochemistry alone may justify escalation, but should not automatically convert the licence as a whole to drill-ready status.

Overall conclusion. The 0.707 High-tier score remains a reasonable screening result and is strengthened, rather than contradicted, by the additional research when it is interpreted correctly: it identifies 41055-HQ-LEL as a licence worth prioritising for disciplined field validation. The next increase in confidence must come from licence-specific ground evidence, not from further amplification of remote-sensing or model-derived confidence.

References

1. Sabins, F. F. (1999). Remote sensing for mineral exploration. Ore Geology Reviews, 14(3–4), 157–183. https://doi.org/10.1016/S0169-1368(99)00007-4

2. Kokaly, R.F., Clark, R.N., Swayze, G.A., Livo, K.E., Hoefen, T.M., Pearson, N.C., Wise, R.A., Benzel, W.M., Lowers, H.A., Driscoll, R.L., and Klein, A.J. (2017). USGS Spectral Library Version 7: U.S. Geological Survey Data Series 1035, 61 p., DOI: 10.3133/ds1035.

3. Beiranvand Pour, A., Zoheir, B., Pradhan, B., & Hashim, M. (Eds.). (2021). Multispectral and Hyperspectral Remote Sensing Data for Mineral Exploration and Environmental Monitoring of Mined Areas. MDPI Books. ISBN: 978-3-0365-1264-8 (Hardback), ISBN: 978-3-0365-1265-5 (PDF). DOI:10.3390/books978-3-0365-1265-5.

4. Beiranvand Pour, A., Parsa, M., & Eldosouky, A. M. (Eds.). (2023). Geospatial analysis applied to mineral exploration: Remote sensing, GIS, geochemical, and geophysical applications to mineral resources. Elsevier.

5. Rowan, L. C., & Mars, J. C. (2003). Lithologic mapping in the Mountain Pass, California area using ASTER data. Remote Sensing of Environment, 84(3), 350–366. https://doi.org/10.1016/S0034-4257(02)00127-X

6. Ministry of Geology of the USSR. (1977). Geological Map of Africa and Arabia (Scale 1:5,000,000). Research Laboratory for Geology of Foreign Countries “NII Zarubezhgeologiya”, Leningrad.

7. Rockwell, B. W. (2012). Description and validation of an automated methodology for mapping mineralogy, vegetation, and hydrothermal alteration type from ASTER satellite imagery with examples from the San Juan Mountains, Colorado. U.S. Geological Survey Scientific Investigations Map 3190, pamphlet 35 p., 5 map sheets, scale 1:100,000. https://doi.org/10.3133/sim3190

8. Clark, R. N., Swayze, G. A., Gallagher, A. J., King, T. V. V., & Calvin, W. M. (1993). The U.S. Geological Survey, Digital Spectral Library: Version 1 (0.2 to 3.0 μm). U.S. Geological Survey Open-File Report 93-592. https://doi.org/10.3133/ofr93592

9. Clark, R. N., Swayze, G. A., Livo, K. E., Kokaly, R. F., Sutley, S. J., Dalton, J. B., McDougal, R. R., & Gent, C. A. (2007). USGS digital spectral library splib06a. U.S. Geological Survey Data Series 231.

10. LeCun, Y., Bengio, Y., & Hinton, G. (2015). Deep learning. Nature, 521(7553), 436–444. https://doi.org/10.1038/nature14539

11. Vaswani, A., Shazeer, N., Parmar, N., Uszkoreit, J., Jones, L., Gomez, A. N., Kaiser, Ł., & Polosukhin, I. (2017). Attention is all you need. Advances in Neural Information Processing Systems (NeurIPS 2017), 5998–6008. (Proceedings PDF) https://papers.neurips.cc/paper/7181-attention-is-all-you-need.pdf

12. Arjovsky, M., Chintala, S., & Bottou, L. (2017). Wasserstein GAN. arXiv preprint arXiv:1701.07875. https://arxiv.org/abs/1701.07875

13. Ma, L., Liu, Y., Zhang, X., Ye, Y., Yin, G., & Johnson, B. A. (2019). Deep learning in remote sensing applications: A meta-analysis and review. ISPRS Journal of Photogrammetry and Remote Sensing, 152, 166–177. https://doi.org/10.1016/j.isprsjprs.2019.04.015

Appendix A: Suggested Reconnaissance Survey Points Coordinates List

Points within the license area

#	Latitude	Longitude	Score
1	15.147772°S	29.074734°E	0.9978
2	15.130285°S	29.119253°E	0.9667
3	15.130124°S	28.997334°E	0.8346
4	15.116423°S	29.066576°E	0.8238
5	15.142084°S	28.916845°E	0.8111
6	15.160021°S	28.812641°E	0.8058
7	15.135804°S	29.092195°E	0.9924
8	15.172673°S	29.072920°E	0.9680
9	15.166352°S	29.049106°E	0.9654
10	15.137677°S	29.066408°E	0.9646
11	15.132277°S	29.100388°E	0.9580
12	15.135524°S	29.083216°E	0.9553
13	15.175130°S	29.082295°E	0.9426
14	15.182127°S	29.072077°E	0.9408
15	15.169548°S	29.135354°E	0.9399
16	15.132738°S	29.128814°E	0.9394
17	15.124056°S	29.085909°E	0.9320
18	15.184789°S	29.059010°E	0.9230
19	15.142259°S	29.041955°E	0.9229
20	15.176022°S	29.064349°E	0.9226
21	15.169168°S	29.059046°E	0.9221
22	15.186272°S	29.035831°E	0.9220
23	15.179613°S	29.049047°E	0.9217

Points outside the license area

#	Latitude	Longitude	Score
1	15.098471°S	29.083042°E	0.8840
2	15.206351°S	29.142458°E	0.8813
3	15.091811°S	29.115693°E	0.8501
4	15.105112°S	29.031877°E	0.8082
5	15.101291°S	29.052781°E	0.8061
6	15.157492°S	28.833380°E	0.7985
7	15.193455°S	29.044879°E	0.9696